Supplementary Information

Enhanced Na Storage Performances through in situ Depolymerization-repolymerization in Bamboo-derived Hard Carbon Anodes

Cong-Cong Li[a,b], Yi-Lin Wang[a], Zong-Lin Yi[a], Fei Yang[a,b], Ruo-Han Niu[a,b], Fang-Yuan Su[a], Yi-Ping Wang[c], Zhi-Fang Liu[c], Zhi-Wei Wu[d]*, Li-Jing Xie[a]*, Cheng-Meng Chen[a,e]*

[a] Shanxi Key Laboratory of Carbon Materials, Institute of Coal Chemistry, Chinese Academy of Sciences, Taiyuan 030001, Shanxi, China

[b] University of Chinese Academy of Sciences, Beijing 100049, China

[c] Hami Hexiang Industry and Trade company with limited liability, Hami 839000, Xinjiang, China

[d] State Key Laboratory of Coal Conversion, Institute of Coal Chemistry, Chinese Academy of Sciences, Taiyuan 030001, Shanxi, China

[e] Center of Materials Science and Optoelectronics Engineering, University of Chinese Academy of Sciences, Beijing 100049, China

*Corresponding authors.

E-mail addresses: wuzhiwei@sxicc.ac.cn (Zhi-Wei Wu)

xielijing@sxicc.ac.cn (Li-Jing Xie)

chencm@sxicc.ac.cn (Cheng-Meng Chen)

Table S1. Fitted parameters of the C 1s spectra of carbon materials.

Element	Assignment	Relative (%)						
		NB	MC-0	MC-9	MC-20	HC-0	HC-9	HC-20
C 1s	sp^2	15.7	51.9	48.2	46.9	86.1	84.5	83.0
	sp^3	40.1	32.4	34.2	35.1	6.3	6.6	7.0
	C–O	32.6	10.7	12.1	13.0	4.8	5.7	6.3
	C=O	11.6	4.9	5.5	5.0	2.9	3.1	3.6

Table S2. Fitted parameters of XRD of MCs.

Samples Units	L_a nm	L_c nm
MC-0	2.293	0.832
MC-9	2.451	0.912
MC-20	2.795	0.940

Table S3. Microcrystalline structure parameters of HCs.

Samples Units	d_{002} nm	L_a nm	L_c nm	I_D/I_G -	$L_{a,\ Raman}$ nm
HC-0	0.3707	3.215	1.044	1.54	12.46
HC-9	0.3708	3.716	1.119	1.39	13.82
HC-20	0.3692	3.930	1.187	1.35	14.28

Table S4. Pore structure parameters of MCs.

Samples Units	$S_{BET}(N_2)$ $m^2\ g^{-1}$	$V_{total}(N_2)$ $cm^3\ g^{-1}$
MC-0	273.1800	0.1488
MC-9	527.4814	0.2639
MC-20	457.4268	0.2368

Table S5. Pore structure parameters of HCs.

Samples Units	$S_{BET}(N_2)$ $m^2\ g^{-1}$	$V_{total}(N_2)$ $cm^3\ g^{-1}$	$S_{BET}(CO_2)$ $m^2\ g^{-1}$	$V_{total}(CO_2)$ $cm^3\ g^{-1}$	Average pore diameter(CO_2) nm
HC-0	2.3966	0.0092	6.4175	0.0011	0.7115
HC-9	31.9511	0.0390	180.5768	0.0445	0.9855
HC-20	20.7420	0.0403	74.4162	0.0174	0.9369

Table S6. Percentage of elemental phosphorus in carbon materials measured by ICP-MS.

Samples Units	Phosphorus content %
MC-0	0.118
HC-0	0.103
MC-9	7.467
HC-9	0.919
MC-20	7.756
HC-20	0.872

Table S7. Atomic content of N 1s and P 2p on the surface of the carbon materials.

Samples	Atomic (%)	
-	N 1s	P 2p
NB	1.26	0.28
MC-0	0.84	0.19
HC-0	0.59	0.31
MC-9	6.07	2.49
HC-9	1.25	0.49
MC-20	6.71	1.96
HC-20	1.26	0.51

Table S8. Fitted parameters of SAXS of HCs.

Samples Units	I_0 -	C_1 -	C_2 -	f_a -	d nm	r_{SAXS} nm
HC-0	6.6399	0.1509	0.0194	0.54	4.90	0.87
HC-9	22.5336	0.4354	0.0780	0.78	10.00	1.48
HC-20	20.3661	0.3881	0.0732	0.72	8.69	1.39

Fitting function：$I_{mp} = I_0 \frac{1}{1 + C_1 Q^2 + C_2 Q^4}$, Where I_0, C_1 and C_2 are adjustable constant parameters.

The average pore radius：$r_{SAXS} = \sqrt{5C_1}$

Amphiphilic factor：$f_a = \frac{C_1}{2\sqrt{C_2}}$

Pore-pore distance：$$d = 2\pi\left[\frac{1}{2}C_2^{-\frac{1}{2}} - \frac{C_1}{4C_2}\right]^{-\frac{1}{2}}$$

Table S9. Fitted parameters of WAXS of HCs.

Samples	A	wL	r	Sigma	xc	D	Σ
Units	-	-	-	-	-	-	-
HC-0	3.9736	7.7348	0.1606	0.4494	17.4727	2.35	0.26
HC-9	1.6639	7.0704	0.0829	3.6071	17.6745	2.83	0.28
HC-20	2.5541	6.5410	0.1189	0.3393	17.7215	2.92	0.31

Fitting function：

$$I_{WAXS} = ((2 * A/pi) * (wL/(4 * (x - xc)\text{^}2 + wL\text{^}2))) * (1 + ((D * D * Sigma\text{^}D)/(r\text{^}D) - 1)/((1 + (x * Sigma)\text{^}2)\text{^}((D - 1)/2)) * sin((D - 1) * atan(x * Sigma))/(x * Sigma)) * (exp(-(x * r)\text{^}2/6) + ((erf(0.306 * x * r))\text{^}6) * (4/(x * r)\text{^}2))$$

, Where A, wL, r, Sigma and xc are adjustable constant parameters.

Bending degree：$$\Sigma = \frac{2}{wL}$$

Table S10. The properties of hard carbons for SIBs reported recently.

Precursor	Reversible capacity	Rate performance	ICE (%)	Source
Bamboo	352.4 mAh g^{-1} at 30 mA g^{-1}	339.8 mAh g^{-1} at 50 mA g^{-1}; 339.4 mAh g^{-1} at 100 mA g^{-1}; 299.2 mAh g^{-1} at 500 mA g^{-1}; 205.8 mAh g^{-1} at 1000 mA g^{-1}	87.6	This work
Bamboo	383.6 mAh g^{-1} at 30 mA g^{-1}	84.9 mAh g^{-1} at 1000 mA g^{-1}	84.5	This work
Forestry biomass	329.3 mAh g^{-1} at 50 mA g^{-1}	90 mAh g^{-1} at 1000 mA g^{-1}	68.8	[1]
Bamboo and CNTs	268.9 mAh g^{-1} at 30 mA g^{-1}	94.7 mAh g^{-1} at 600 mA g^{-1}	-	[2]
Phellem	330.0 mAh g^{-1} at 20 mA g^{-1}	225.0 mAh g^{-1} at 500 mA g^{-1}; 205.5 mAh g^{-1} at 1000 mA g^{-1}	90.0	[3]
Cellulose	239.0 mAh g^{-1} at 25 mA g^{-1}	175.0 mAh g^{-1} at 1000 mA	83.0	[4]

Coconut shell	343 mAh g^{-1} at 30 mA g^{-1}	178.0 mAh g^{-1} at 1500 mA g^{-1}	69.8	5
Almond shells	309.9 mAh g^{-1} at 50 mA g^{-1}	235.4 mAh g^{-1} at 1000 mA g^{-1}	87.2	6
Furfural residues	302.5 mAh g^{-1} at 20 mA g^{-1}	70.0 mAh g^{-1} at 1000 mA g^{-1}	90.9	7
Olive shell	313.0 mAh g^{-1} at 50 mA g^{-1}	90.0 mAh g^{-1} at 1000 mA g^{-1}	78.0	8
Bamboo fibers	338.0 mAh g^{-1} at 50 mA g^{-1}	228.0 mAh g^{-1} at 1000 mA g^{-1}	75.0	9

Table S11. R_{ct}, Conductivity, and Resistivity of HCs.

Samples Units	R_{ct} Ω	Conductivity S cm^{-1}	Resistivity Ω cm^{-1}
HC-0	4.569	25.947	0.039
HC-9	2.719	27.122	0.037
HC-20	2.366	28.277	0.035

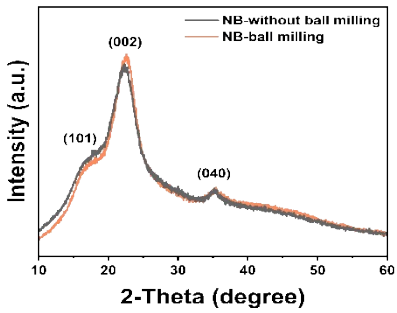

Fig. S1. XRD patterns.

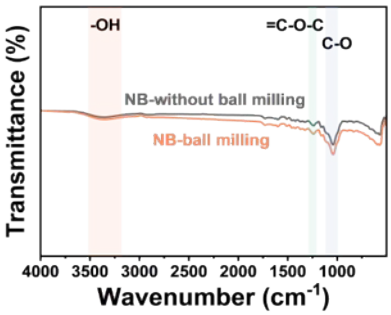

Fig. S2. FT-IR spectra.

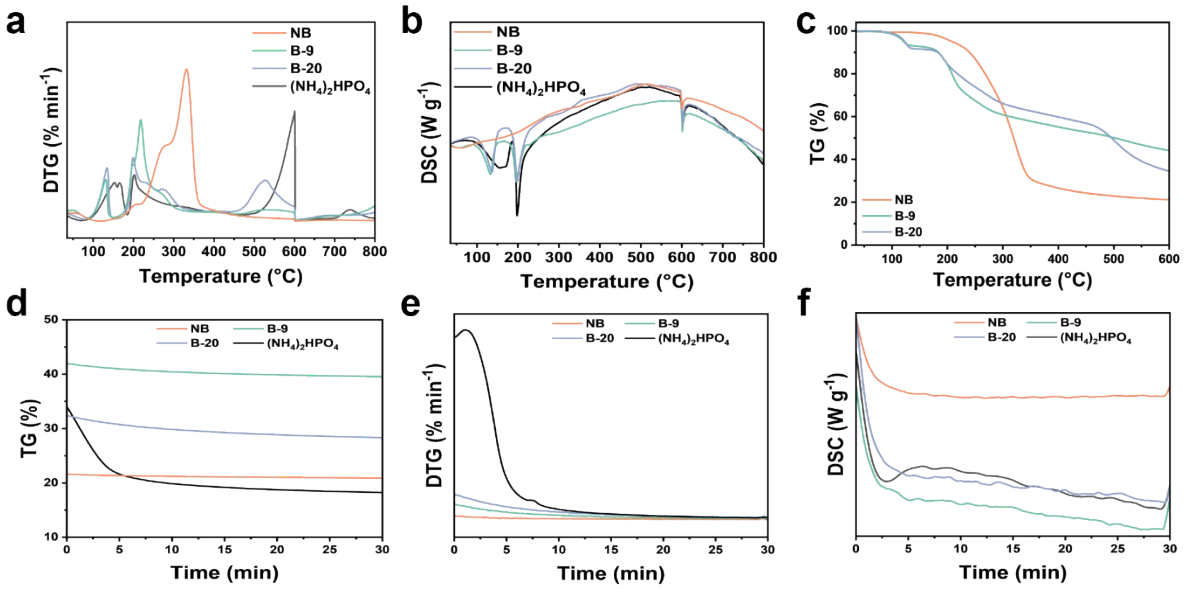

Fig. S3. (a) DTG, (b) DSC, and (c) TG in TG-MS. (d-f) TG, DTG, DSC images held at 600 °C for 30 minutes.

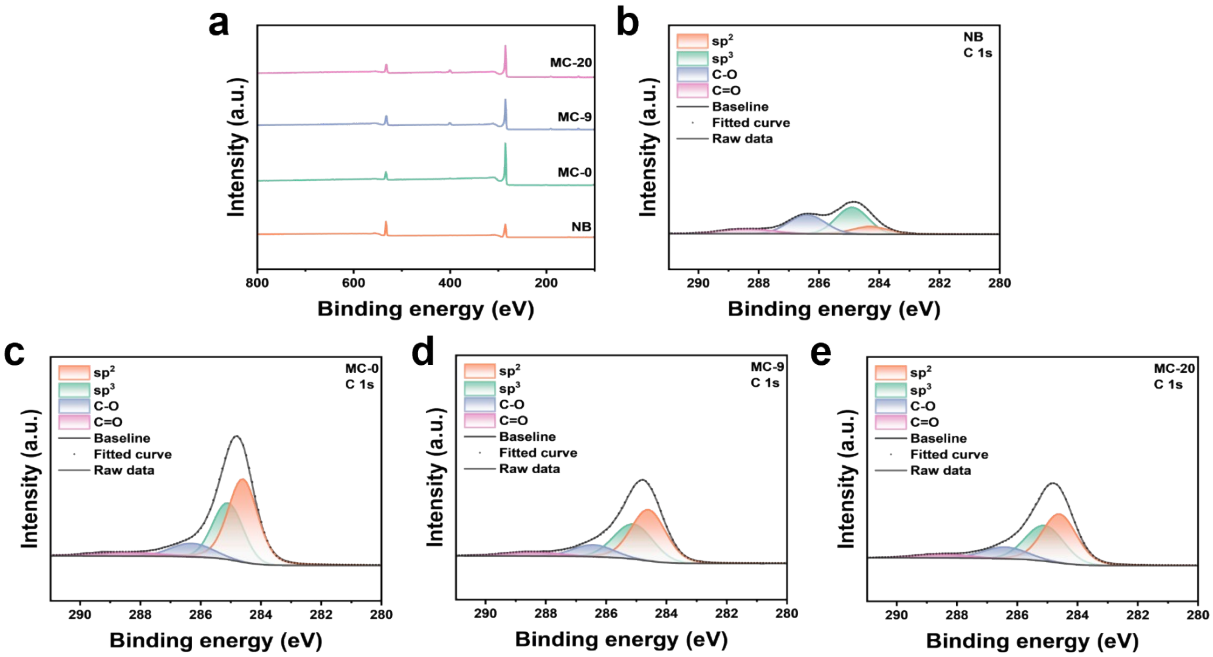

Fig. S4. (a) XPS spectra. C 1s spectra peak fitting of (b) NB, (c) MC-0 (d) MC-9 and (e) MC-20.

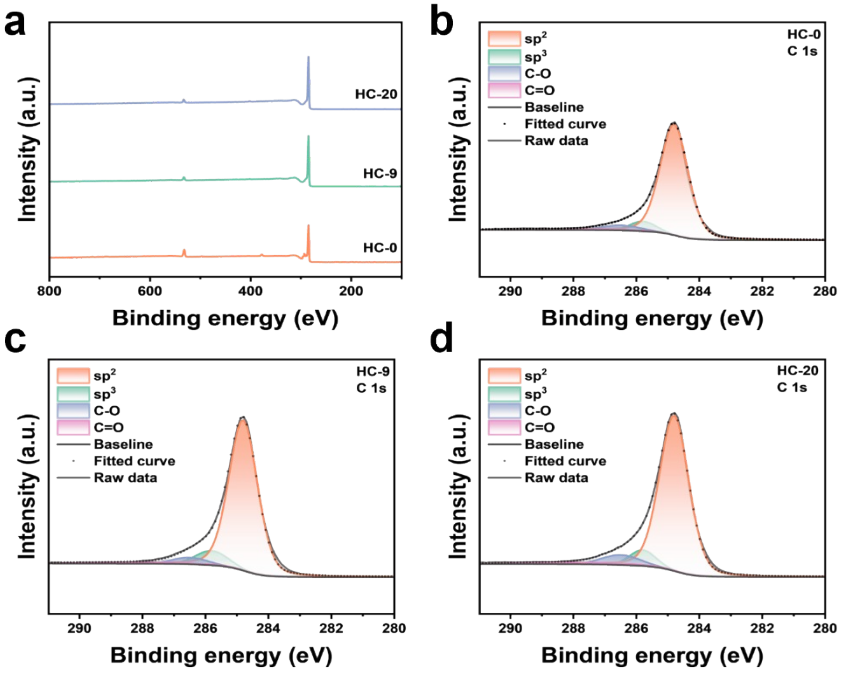

Fig. S5. (a) XPS spectra. C 1s spectra peak fitting of (b) HC-0, (c) HC-9, and (d) HC-20.

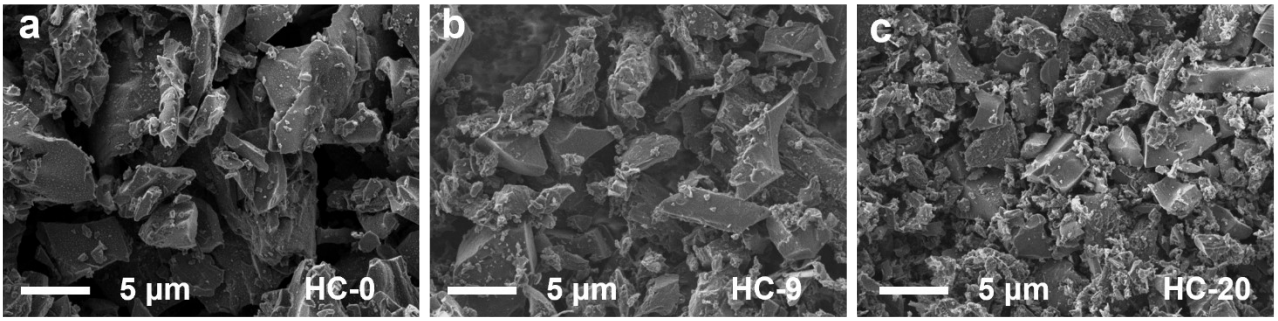

Fig. S6. SEM images of HCs.

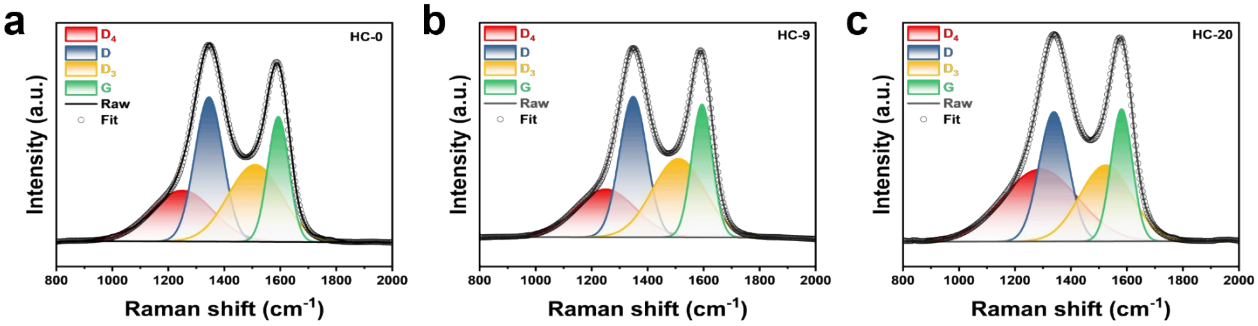

Fig. S7. Fitted Raman spectra of HCs.

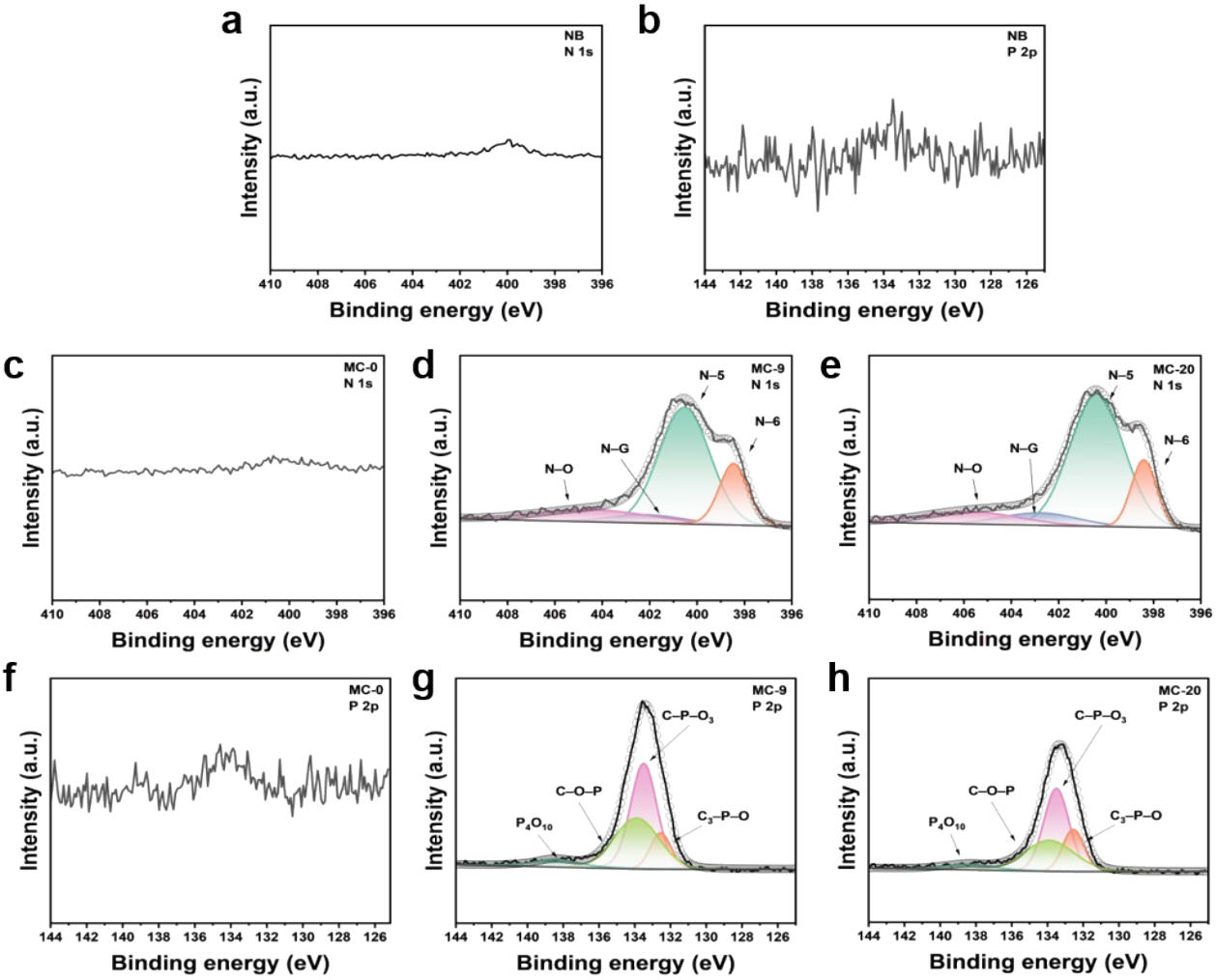

Fig. S8. N 1s and P 2p spectra peak fitting of NB, MC-0, MC-9, and MC-20.

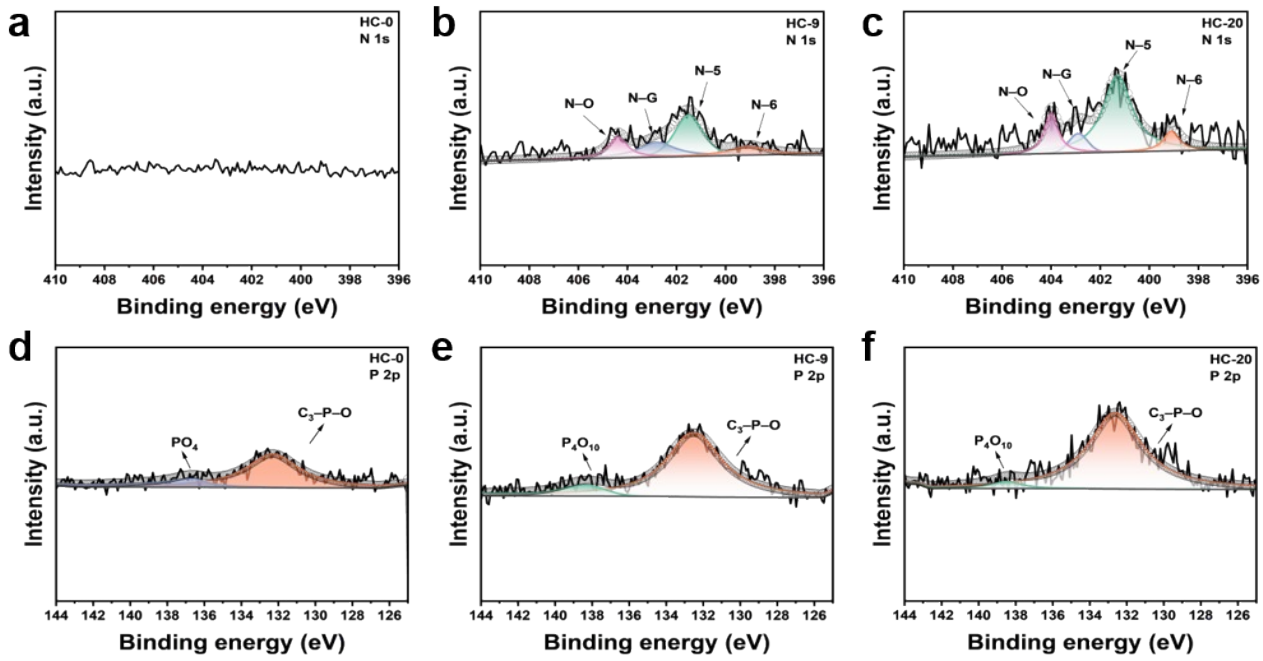

Fig. S9. N 1s and P 2p spectra peak fitting of HC-0, HC-9, and HC-20.

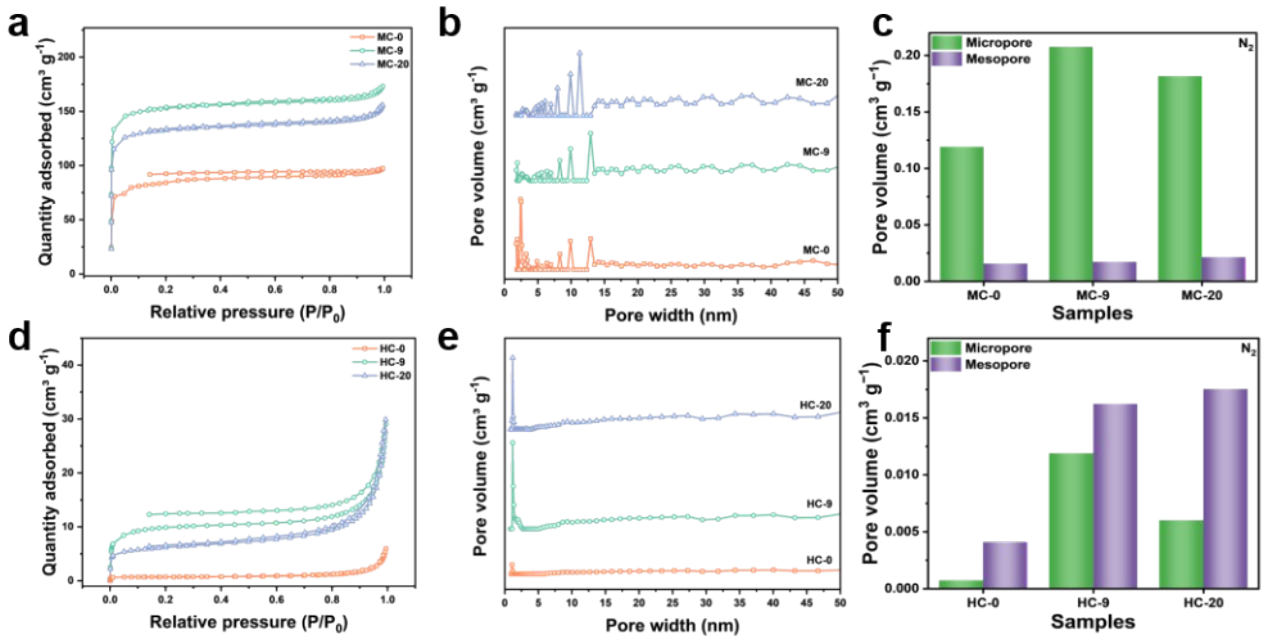

Fig. S10. (a, d) N_2 adsorption−desorption isotherms. (b, e) The pore size distribution (N_2). (c, f) Micropore volume and mesopore volume (N_2) of carbon materials.

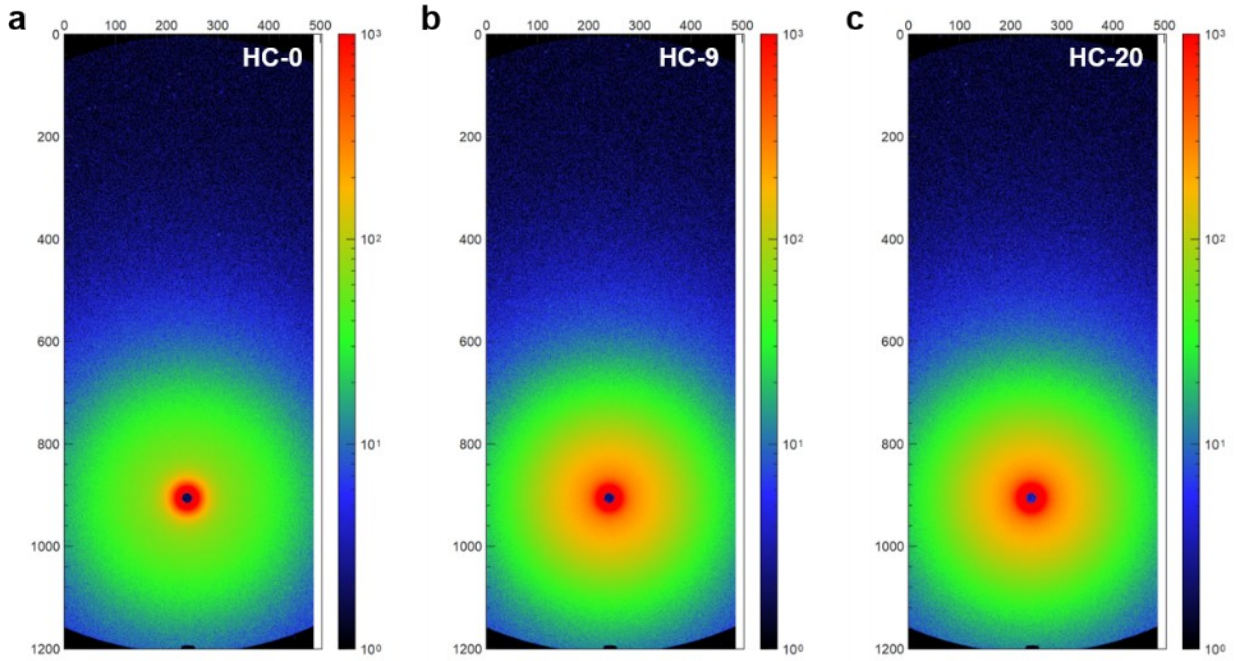

Fig. S11. Two-dimensional pattern of small-angle X-ray scattering.

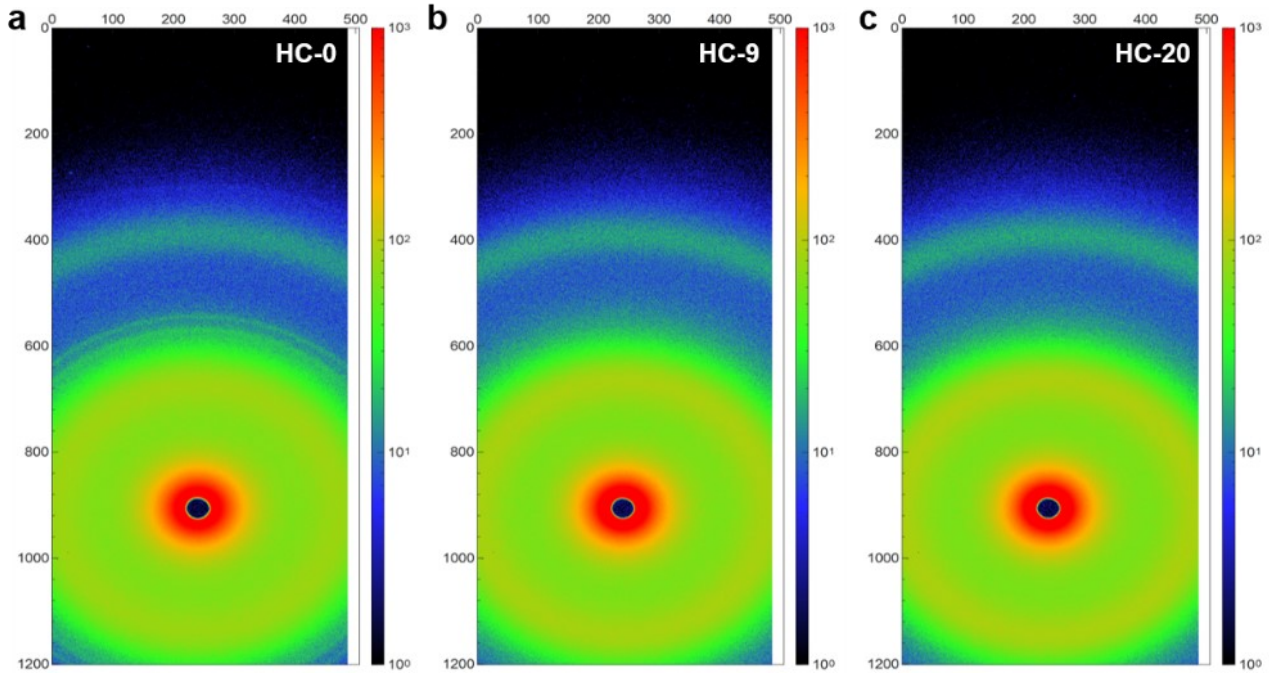

Fig. S12. Two-dimensional pattern of wide-angle X-ray scattering.

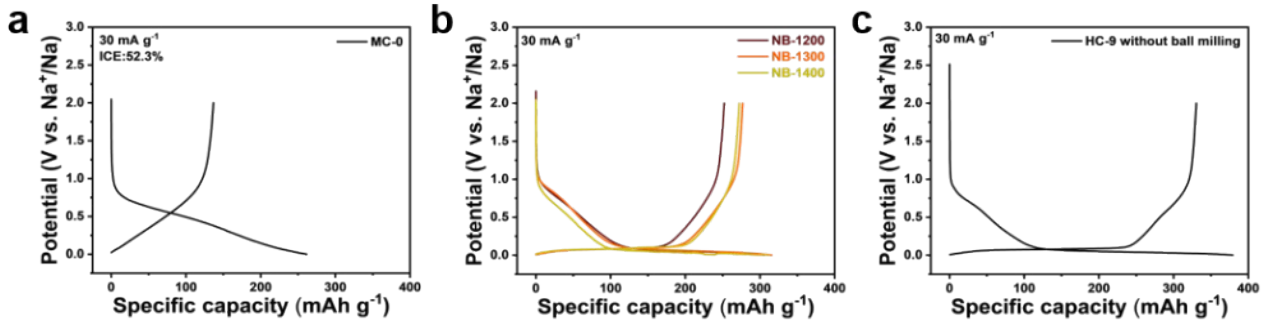

Fig. S13. Initial galvanostatic discharge/charge profiles at 30 mA g^{-1}.

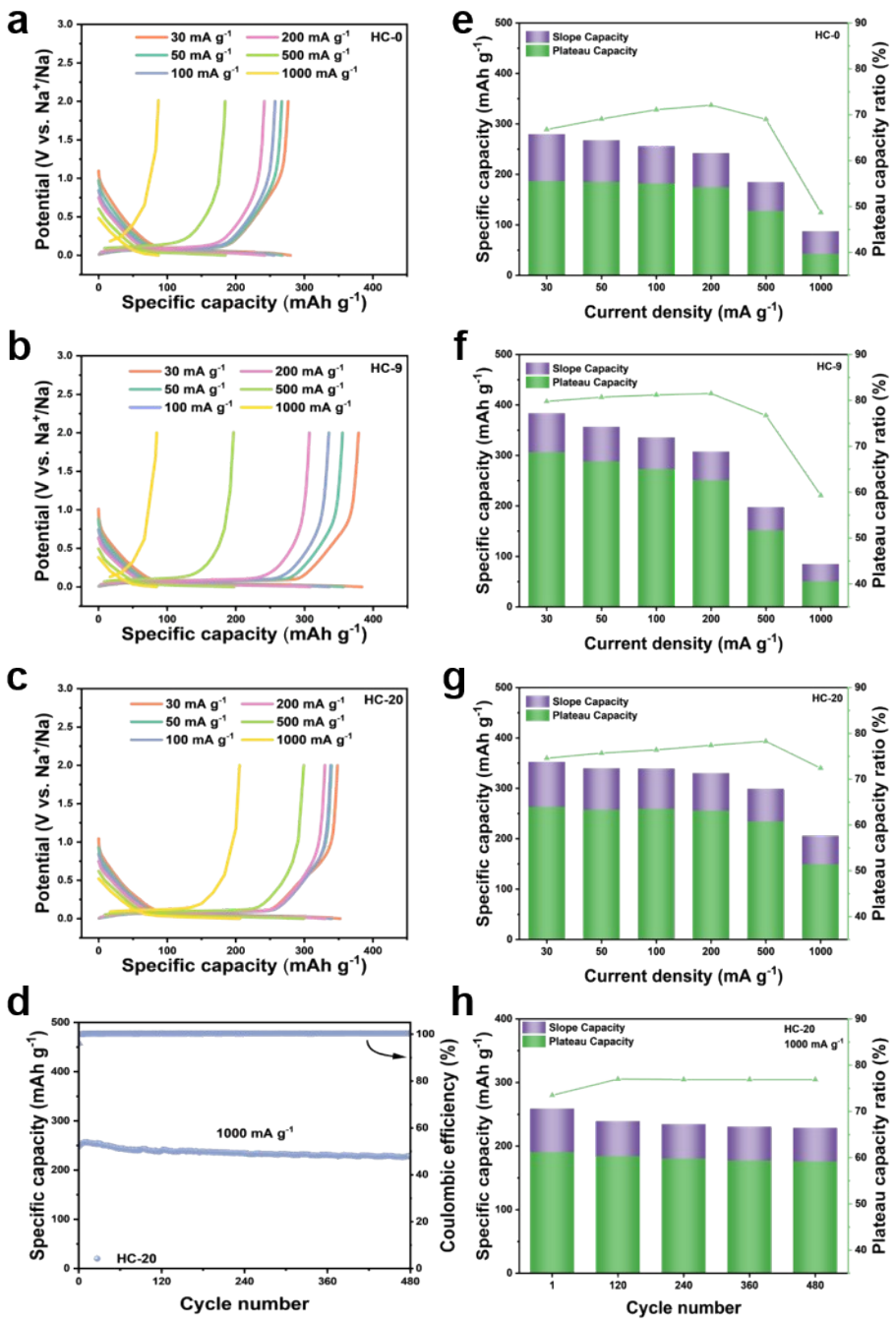

Fig. S14. (a-c) Galvanostatic discharge/charge profiles at different current density. (d) Cycling performance of HC-20 at 1000 mA g^{-1}. (e-g) The plateau and slope capacity distribution below and above 0.1 V and plateau capacity ratio. (h) The capacity of HC-20 in the plateau area, slope area and the proportion of plateau area capacity in different cycles.

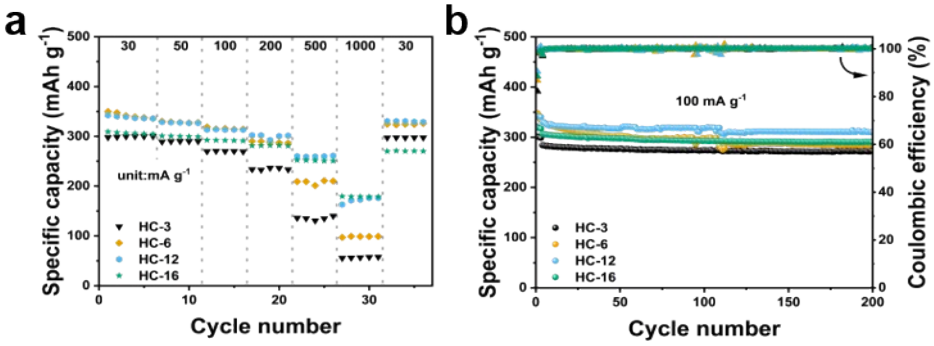

Fig. S15. (a)Rate performance. (b)Cycle performance at 100 mA g^{-1}.

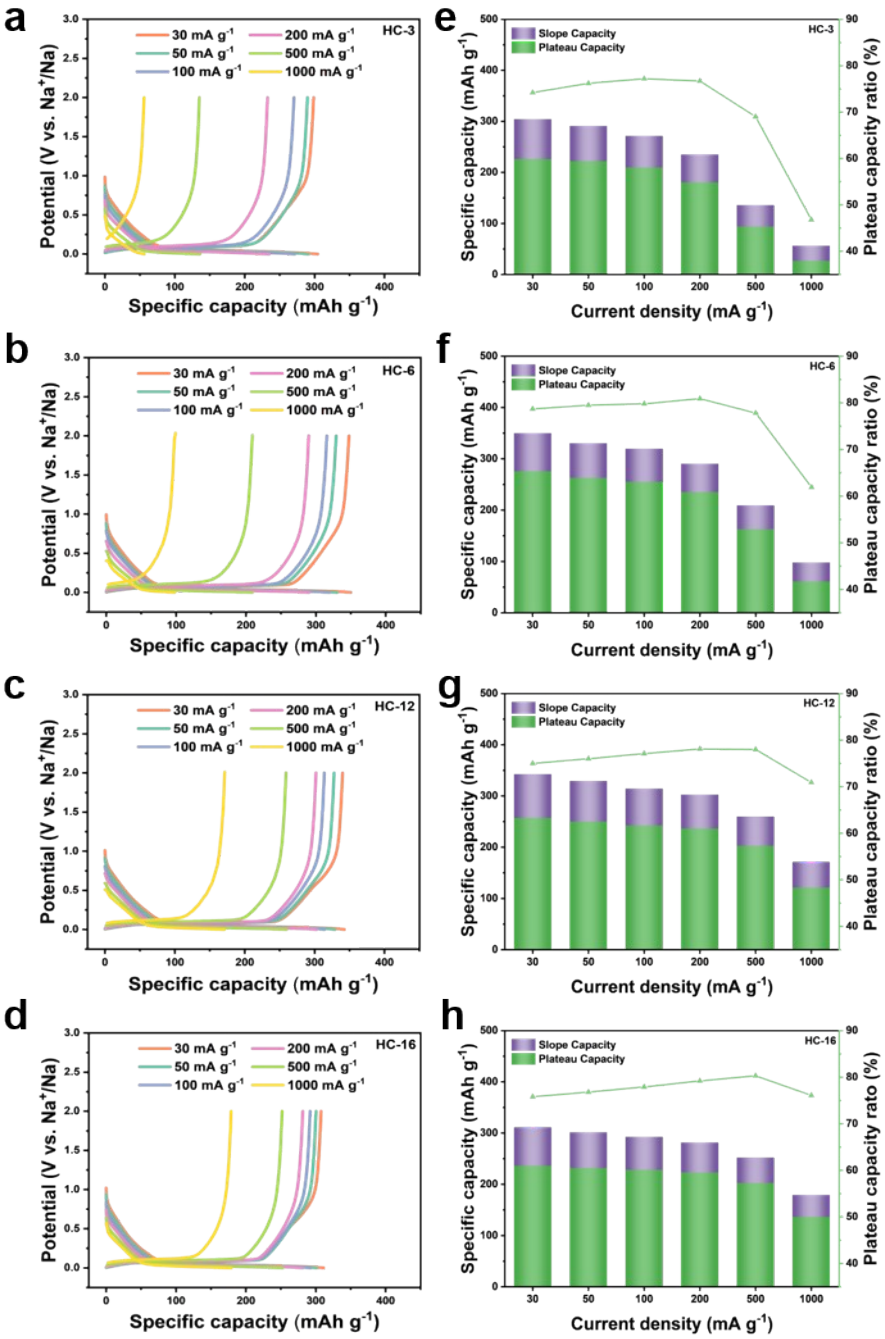

Fig. S16. (a-d) Galvanostatic discharge/charge profiles at different current density. (e-h) The plateau and slope capacity distribution below and above 0.1 V and plateau capacity ratio.

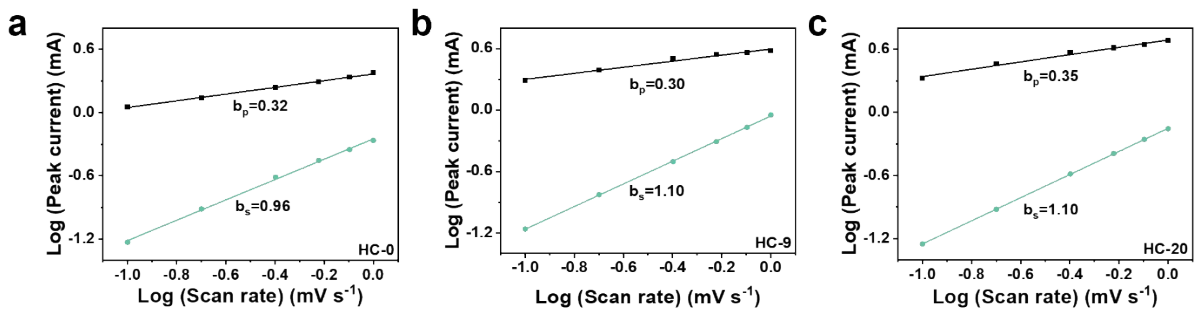

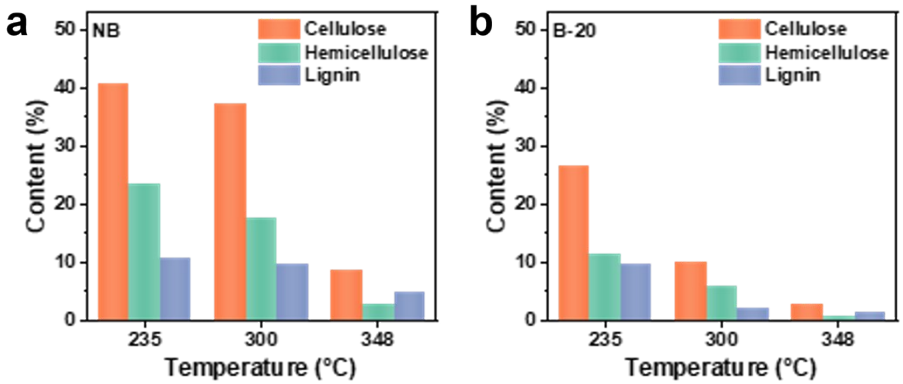

Fig. S17. The relationship of log-peak current and log-scan scan of HC-0, HC-9 and HC-20.

Fig. S18. The content of cellulose, hemicellulose, and lignin in NB and B-20 at 235, 300 and 348°C.

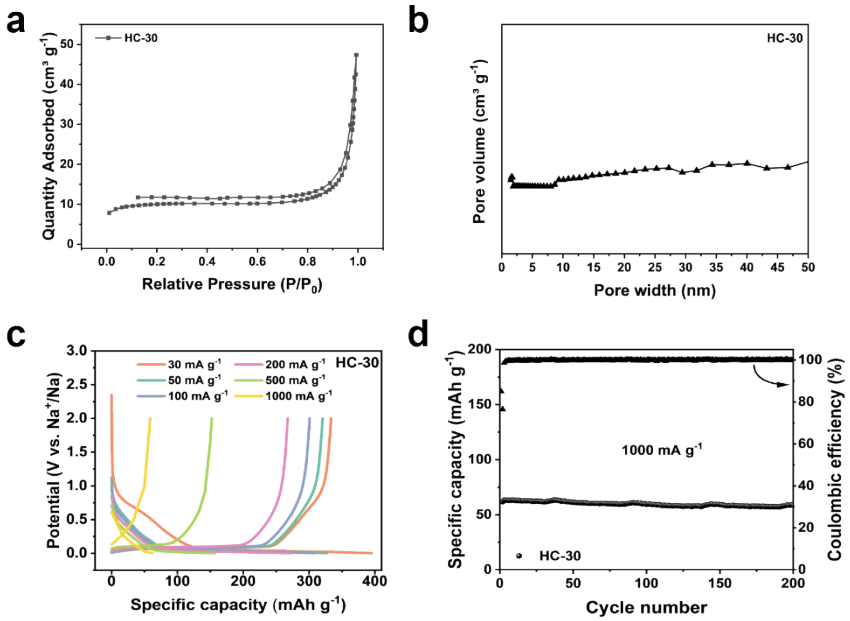

Fig. S19. (a) N_2 adsorption-desorption isotherms of HC-30. (b) The pore size distribution (N_2) of HC-30. (c) Galvanostatic discharge/charge profiles of HC-30 at different current density. (d) Long cycle performance at 1000 mA g^{-1}.

$$(NH_4)_2HPO_4(s) \xrightarrow{432K} 2NH_3(g) + H_3PO_4(l) \qquad (1)$$

$$(NH_4)_2HPO_4(s) \xrightarrow{432K} NH_3(g) + (NH_4)H_2PO_4(s) \qquad (2)$$

$$(NH_4)H_2PO_4(s) \xrightarrow{432K} NH_3(g) + H_3PO_4(l) \qquad (3)$$

$$2H_3PO_4(l) \xrightarrow{432K\text{，}482K} H_2O(g) + H_4P_2O_7(l) \qquad (4)$$

$$2H_4P_2O_7(l) \xrightarrow{>482K} 4H_2O(g) + P_4O_{10}(s) \qquad (5)$$

Scheme 1. Decomposition equation of $(NH_4)_2HPO_4$.

Calculation S1. Calculation Method of g value

$$g = \frac{hv}{\beta H}$$

In this formula, h is the Plank constant, v is the microwave frequency of X-band spectrometer(v = 9.83 GHz), β is the electron Bohr magneto, H is the applied magnetic field.

Calculation S2. Calculation Method of L_a and L_c

$$L_a \& L_c = \frac{\kappa\lambda}{\beta\cos\theta}$$

In this formula, κ is scherrer constant (κ is 1.84 for L_a and κ is 0.9 for L_c), λ is the radiation wavelength (λ = 1.5418 Å), β is the half-height width of the (002) peak, θ is the reflection angle of (002) or (100).

$$L_{a,\,Raman} = (2.4 \times 10^{-10})\lambda^4(I_G/I_D)$$

In this formula, λ is 532 nm.

Calculation S3. Calculation Method of b-value

$$i = av^b$$

where a and b are constants, and b can be estimated from the slope curve plotted between log(v) and log(i). The b value of 0.5 indicates a diffusion-controlled process, whereas the b value of 1 indicates a surface-controlled reaction. Considering the potential deviation from the equilibrium potential due to the irreversible resistance, we take points based on the potential deviation around 0.01 V and 0.5 V.

Calculation S4. Calculation Method of capacitive contribution

$$i(V) = k_1 v + k2v^{1/2}$$

Where $i(V)$ stands for the current at a specific potential, v stands for the scan rate, and $k_1 v$ and $k2v^{1/2}$ stands for the surface-controlled and diffusion-controlled capacities, respectively.

Calculation S5. Calculation Method of the Apparent Na^+ Diffusion Coefficient

$$D_{Na^+} = \frac{4}{\pi\tau}\left(\frac{m_B V_M}{M_B S}\right)\left(\frac{\Delta E_S}{\Delta E_\tau}\right)^2$$

where τ, m_B, V_M, and S are the pulse duration, mass of the active material, molar volume, active surface area, respectively. ΔE_S is the difference between the stable potentials and ΔEτ is the instantaneous total voltage change of the constant current battery at τ.

References

1 G. Zhang, C. Chen, C. Xu, J. Li, H. Ye, A. Wang, X. Cao, K. Sun and J. Jiang, *Energy Fuel*, 2024, **38**, 8326–8336.

2 S. Pothaya, C. Poochai, N. Tammanoon, Y. Chuminjak, T. Kongthong, T. Lomas, C. Sriprachuabwong and A. Tuantranont, *Rare Met.*, 2024, **43**, 124–137.

3 S. Zhou, Z. Tang, G. Jin, J. Tu, A. S. Dhmees, Y. Tang, D. Sun, R. Zhang and H. Wang, *Small*, 2024, **20**, 2407341.

4 Y.-J. Xu, Y.-Y. Wang, Z.-Y. Gu, C.-S. Zhao, X.-L. Wu, S. R. P. Silva and B.-H. Hou, *Energy Stor. Mater.*, 2025, **75**, 104031.

5 J. Xiang, L. Ma, Y. Sun, S. Dong, Q. Xu, X. He, Y. Zhou and C. Hai, *Langmuir*, 2024, **40**, 23853–23863.

6 X. Li, S. Zhang, J. Tang, J. Yang, K. Wen, J. Wang, P. Wang, X. Zhou and Y. Zhang, *J. Mater. Chem. A*, 2024, **12**, 21176–21189.

7 X. Guo, Z. Zhang, Y. Wang, X. Tian, Y. Qiao and P. Han, *J. Power Sources*, 2025, **625**, 235664.

8 L. Zhou, Y. Cui, P. Niu, L. Ge, R. Zheng, S. Liang and W. Xing, *Carbon*, 2025, **231**, 119733.

9 Z. Huang, J. Huang, L. Zhong, W. Zhang and X. Qiu, *Small*, 2024, 2405632.